A Mutational Analysis of Binding Interactions in an Antigen−Antibody Protein−Protein Complex†

William Dall'Acqua,[§,||,⊥] Ellen R. Goldman,[§,⊥] Wenhong Lin,[§] Connie Teng,[§] Daisuke Tsuchiya,[§] Hongmin Li,[§] Xavier Ysern,[#] Bradford C. Braden,[§,▽] Yili Li,[○] Sandra J. Smith-Gill,[○] and Roy A. Mariuzza*[,§]

Center for Advanced Research in Biotechnology, University of Maryland Biotechnology Institute, 9600 Gudelsky Drive, Rockville, Maryland 20850, Center for Drug Evaluation and Research, U.S. Food and Drug Administration, 5600 Fishers Lane, Rockville, Maryland 20857, Bowie State University, Bowie, Maryland 20715, and National Cancer Institute, National Institutes of Health, Bethesda, Maryland 20892

Received January 20, 1998; Revised Manuscript Received March 16, 1998

ABSTRACT: Alanine scanning mutagenesis, double mutant cycles, and X-ray crystallography were used to characterize the interface between the anti-hen egg white lysozyme (HEL) antibody D1.3 and HEL. Twelve out of the 13 nonglycine contact residues on HEL, as determined by the high-resolution crystal structure of the D1.3−HEL complex, were individually truncated to alanine. Only four positions showed a $\Delta\Delta G$ ($\Delta G_{mutant} - \Delta G_{wild-type}$) of greater than 1.0 kcal/mol, with HEL residue Gln121 proving the most critical for binding ($\Delta\Delta G = 2.9$ kcal/mol). These residues form a contiguous patch at the periphery of the epitope recognized by D1.3. To understand how potentially disruptive mutations in the antigen are accommodated in the D1.3−HEL interface, we determined the crystal structure to 1.5 Å resolution of the complex between D1.3 and HEL mutant Asp18 → Ala. This mutation results in a $\Delta\Delta G$ of only 0.3 kcal/mol, despite the loss of a hydrogen bond and seven van der Waals contacts to the Asp18 side chain. The crystal structure reveals that three additional water molecules are stably incorporated in the antigen−antibody interface at the site of the mutation. These waters help fill the cavity created by the mutation and form part of a rearranged solvent network linking the two proteins. To further dissect the energetics of specific interactions in the D1.3−HEL interface, double mutant cycles were carried out to measure the coupling of 14 amino acid pairs, 10 of which are in direct contact in the crystal structure. The highest coupling energies, 2.7 and 2.0 kcal/mol, were measured between HEL residue Gln121 and D1.3 residues V_LTrp92 and V_L-Tyr32, respectively. The interaction between Gln121 and V_LTrp92 consists of three van der Waals contacts, while the interaction of Gln121 with V_LTyr32 is mediated by a hydrogen bond. Surprisingly, however, most cycles between interface residues in direct contact in the crystal structure showed no significant coupling. In particular, a number of hydrogen-bonded residue pairs were found to make no net contribution to complex stabilization. We attribute these results to accessibility of the mutation sites to water, such that the mutated residues exchange their interaction with each other to interact with water. This implies that the strength of the protein−protein hydrogen bonds in these particular cases is comparable to that of the protein−water hydrogen bonds they replace. Thus, the simple fact that two residues are in direct contact in a protein−protein interface cannot be taken as evidence that there necessarily exists a productive interaction between them. Rather, the majority of such contacts may be energetically neutral, as in the D1.3−HEL complex.

A detailed knowledge of the molecular basis of protein−protein recognition is an essential element in understanding protein function, since the ability of proteins to form specific complexes with other proteins underlies most cellular processes. X-ray crystallographic studies of protein−protein complexes have provided much valuable information on the molecular architecture of protein−protein interfaces, including the identity of contact residues, the amount of buried surface area, the number and type of hydrogen bonds and van der Waals contacts, and the magnitude of conformational changes associated with complex formation (*1*−*4*). However, the relative contributions of surface complementarity, hydrophobicity, and hydrogen bonding to the energetics of binding, as well as the role of bound water molecules in complex stabilization, remain to be elucidated. Furthermore, the structural and functional consequences of specific amino acid substitutions in a protein−protein interface are still difficult to predict (*5*−*7*). Finally, the number, nature, and location of interface residues that actively participate in complex formation are an important issue; this has given rise to the notion of "functional" or "energetic" epitopes

† This work was supported by NIH Grant GM5280 and the Lucille P. Markey Charitable Trust.

‡ Atomic coordinates have been deposited in the Brookhaven Data Bank as entry 1A2Y.

* To whom correspondence should be addressed. Tel: 301-738-6243. Fax: 301-738-6255. E-mail: mariuzza@indigo2.carb.nist.gov.

§ University of Maryland Biotechnology Institute.

|| Present address: Department of Molecular Oncology, Genentech Inc., 1 DNA Way, South San Francisco, CA 94080.

⊥ These authors contributed equally to this work.

Center for Drug Evaluation and Research.

▽ Bowie State University.

○ National Cancer Institute.

S0006-2960(98)00148-2 CCC: $15.00 © 1998 American Chemical Society
Published on Web 05/14/1998

defined by those contact residues accounting for most of the binding energy. Some authors have described different classes of functional epitopes (*8*−*10*) and questioned the widely held view that protein−protein association is invariably mediated by only a few strong noncovalent interactions (*11*−*14*). This highlights the complexity of protein−protein association processes and serves as a warning against temptations to generalize them. It is therefore apparent that further structure−function studies are required in order to progress from purely anatomical descriptions of protein−protein interfaces to a precise understanding of how structural features contribute to the affinity and specificity of binding reactions.

Antigen−antibody complexes represent excellent models for studying the structure and energetics of protein−protein interactions (*5*, *6*, *15*−*17*). We have developed two independent, yet related, systems for this purpose: (1) the complex between the bacterially expressed Fv fragment (a heterodimer consisting of only the light and heavy chain variable regions, V_L and V_H) of the anti-hen egg white lysozyme (HEL)[1] antibody D1.3 and HEL and (2) the complex between FvD1.3 and the Fv fragment of the anti-D1.3 antibody E5.2. The crystal structures of the FvD1.3−HEL and FvD1.3−FvE5.2 complexes have been determined to 1.8 and 1.9 Å resolution, respectively (*18*−*20*). In addition, site-directed mutants of FvD1.3 and FvE5.2 can be readily produced as secreted proteins in the periplasmic space of *Escherichia coli* and their affinities measured by surface plasmon resonance detection, equilibrium sedimentation, or titration calorimetry.

We previously analyzed the relative contributions of individual residues of D1.3 to binding HEL and E5.2 by alanine scanning mutagenesis and showed that the functionally important residues of D1.3 are different for binding these two proteins, even though D1.3 contacts HEL and E5.2 through essentially the same set of combining site residues (and most of the same atoms) (*8*). Thus, the same protein may recognize different ligands in ways that are structurally similar yet energetically distinct. To further map the D1.3−E5.2 interface, double mutant cycles (*21*−*23*) were carried out to measure the coupling energies ($\Delta\Delta G_{int}$) between specific residue pairs (*9*). The highest $\Delta\Delta G_{int}$ (4.3 kcal/mol) was measured for a charged-neutral pair that forms a buried hydrogen bond, while side chains that interact through solvated hydrogen bonds had lower values (1.3−1.7 kcal/mol). Interaction energies of similar magnitude (1.3−1.6 kcal/mol) were measured for residues forming only van der Waals contacts. These results were broadly consistent with expectations based on the three-dimensional structure of the FvD1.3−FvE5.2 complex.

In the current study, we have extended our analysis of binding interactions in the D1.3−HEL interface by site-directed mutagenesis and X-ray crystallography to include mutants of the antigen. A previous limitation of the FvD1.3−HEL system was the lack of an efficient method for expressing HEL mutants in secreted form in bacteria, as for FvD1.3 and FvE5.2. We have now produced such mutants by in vitro refolding from bacterial inclusion bodies, as well as by secretion in yeast. Twelve nonglycine residues of HEL in contact with D1.3 were individually mutated to alanine and the affinities of the mutants for D1.3 determined using surface plasmon resonance detection. We show that the energetics of binding to the antibody are dominated by only a small subset of HEL residues tested (2 of 12). This is similar to the D1.3 side of the interface where only 3 out of 13 contact residues contribute significantly to binding HEL. In contrast, the binding of E5.2 by D1.3 is mediated by a much larger subset of D1.3 residues (11 of 15) in contact with E5.2 in the crystal structure (*8*). Thus, the D1.3−HEL interface, unlike that between D1.3 and E5.2, is remarkably tolerant to mutations. To understand how potentially destabilizing mutations are accommodated in the D1.3−HEL interface, we determined the crystal structure to 1.5 Å resolution of the complex between FvD1.3 and a mutant of HEL, Asp18 → Ala. Although this mutation results in the loss of a hydrogen bond and a number of van der Waals contacts to the Asp18 side chain, the affinity of the mutant for D1.3 is nearly identical to that of wild-type HEL. The crystal structure reveals a rearrangement of solvent structure at the site of the mutation, but no significant changes in protein structure. To further dissect the energetics of the FvD1.3−HEL interface, double mutant cycles were constructed for 10 residue pairs in direct contact in the crystal structure. In contrast to the D1.3−E5.2 interface in which nearly all residues within 4 Å of each other had coupling energies exceeding 1.0 kcal/mol, most contacting residues in the D1.3−HEL interface showed no significant coupling. These included residue pairs forming hydrogen bonds which, on the basis of donor−acceptor distance and relative orientation of the interacting groups, were expected to be strong. The reasons for the marked differences between actual and expected coupling energies for these residue pairs are discussed in terms of the theory of double mutant cycles and the high-resolution crystal structure of mutant FvD1.3−HEL complexes.

MATERIALS AND METHODS

Reagents. All chemicals were of analytical grade. Restriction enzymes and DNA-modifying enzymes were purchased from New England Biolabs, Inc. (Beverly, MA). Oligonucleotides were synthesized on a 380B DNA synthesizer (Applied Biosystems, Foster City, CA). Radiolabeled [^{35}S]dATP was obtained from Amersham Corp.

Production of Wild-Type and Mutant Fv Fragments. The single-chain version of FvD1.3 (scFvD1.3; *24*) and of the mutants was expressed in *E. coli* BMH 71-18 cells as previously described (*8*). The scFv fragments were purified from culture supernatants by affinity chromatography using either the anti-D1.3 antibody E5.2 or HEL coupled to Sepharose 4B. Prior to BIAcore analysis, all scFv fragments were further purified by size exclusion chromatography on a Superose 12 column (Pharmacia, Uppsala, Sweden) in 0.2 M sodium phosphate, pH 7.4, to eliminate aggregated material which could interfere with affinity measurements (*25*).

In Vitro Refolding of HEL Mutants from Bacterial Inclusion Bodies. A cDNA encoding HEL inserted into the pSP72 cloning vector was kindly provided by Dr. José Moreno-

[1] Abbreviations: HEL, hen egg white lysozyme; scFv, single chain Fv fragment; PBS, phosphate-buffered saline; RU, resonance units; CDR, complementarity-determining region; V_L, light-chain variable region; V_H, heavy-chain variable region.

Rodriguez (Centro Medico National Siglo XXI IMSS, Mexico City). Two *Nde*I sites were introduced at the 5′ and 3′ ends of the HEL gene by the polymerase chain reaction, using the primers 5′-GGGAATTCCATATGAAAGTCTTTG-GAC-3′ and 5′-TTCCCAAGCATATGTTATTACAGACG-GCAACC-3′ (*Nde*I sites underlined), to permitted cloning into the pET11a expression vector (Stratagene, La Jolla, CA) as an *Nde*I fragment. The sequence was verified by the dideoxynucleotide sequencing method (*26*) using a Sequenase Version 2.0 Kit (USB, Cleveland, OH).

E. coli strain BL21(DE3) was transformed with constructs expressing the different HEL mutants. Fresh transformants were always used for protein production. A 10 mL preculture in Luria-Bertani medium containing 100 μg/mL ampicillin was grown at 37 °C under agitation to an absorbance of 1.0 at 600 nm. This preculture was then used to inoculate 500 mL of LB containing 100 μg/mL ampicillin. The bacteria were grown at 37 °C to an absorbance of 1.0, and isopropyl β-D-thiogalactoside was added to a final concentration of 1 mM. After 2 h of further incubation, the bacteria were pelleted and frozen at −70 °C. The frozen cells were resuspended in 25 mL of 50 mM Bis-Tris, pH 6.0, and passed through a French press twice at 1300 psi. The lysate was centrifuged for 15 min at 10 000 rpm and the pellet washed twice with 25 mL of Bis-Tris buffer. Each wash consisted of resuspending the pellet and then centrifuging 10 min at 10 000 rpm. The final pellet was resuspended in 1 mL of the Bis-Tris buffer, layered on a solution of 50% sucrose (w/v) in Bis-Tris, and spun in an ultracentrifuge for 1 h at 30 000 rpm. After centrifugation, the sucrose solution was discarded and the pellet washed twice with 25 mL Bis-Tris buffer, twice with 25 mL of a solution of 0.5% (v/v) Triton X-100, 1 mM EDTA, and 50 mM DTT in Bis-Tris, and a final two times with Bis-Tris alone. The pellet was resuspended in 15 mL of buffer A (8 M urea and 50 mM DTT in Bis-Tris buffer), put under a nitrogen atmosphere, sealed, and agitated overnight with a magnetic stirrer.

The next day the mix was transferred into microfuge tubes and centrifuged for 10 min. The supernatant was loaded at room temperature under gravity onto a 3 mL S-Sepharose (Pharmacia) column which had been equilibrated with buffer A. After loading, the column was washed with 40 mL of buffer A and eluted with a gradient of buffer B (buffer A containing 0.5 M NaCl). Thirteen 1.5 mL fractions were collected, and the absorbance at 280 nm was measured to identify protein-containing fractions; HEL mutants usually eluted in fractions 6−10. The peak fractions were combined so as not to exceed 1 mg/mL ($\epsilon = 2.37$ mL/mg for denatured HEL; *27*). Three hundred milliliters of a renaturation mix (3 M sarcosine, 4 M urea, 0.1 M Tris-HCl, pH 8.0, 1 mM EDTA, 3 mM reduced glutathione, and 0.3 mM oxidized glutathione) was prepared, filtered, and prewarmed to 40 °C for each preparation (*28*). The purified, denatured mutant HEL was added dropwise to the renaturation buffer under vigorous agitation to a final concentration of not more than 0.02 mg/mL. The renaturation mix was incubated at 40 °C overnight and then dialyzed extensively against phosphate-buffered saline (PBS) at 4 °C; the dialysis bags were inverted every few hours to homogenize the mixture. The protein solution was concentrated from about 600 mL after dialysis to 1 mL, using first an Amicon 8200 and then a Millipore Ultrafree-15 (Bedford, MA) concentrator. Each HEL preparation was tested for lysozyme activity using *Micrococcus lysodeikticus* cells from Sigma (St. Louis, MO) according to Charlemagne and Jolles (*29*). Refolded HEL mutants were further purified on a Mono S cation-exchange FPLC column (Pharmacia) equilibrated with 50 mM MES, pH 6.5, and developed with a linear NaCl gradient. All mutants eluted as two major peaks between 0.3 and 0.4 M NaCl. The peaks had lysozyme activities indistinguishable from that of commercial HEL and behaved identically in BIAcore experiments. Refolding yields were typically 2−5%.

Site-Directed Mutagenesis. Mutagenesis of HEL was carried out after subcloning the gene as an *Xba*I/*Hin*dIII fragment into M13mp19 as described (*30*) with a Muta-Gene M13 in vitro Mutagenesis Kit (Bio-Rad, Richmond, CA). Mutagenic oligonucleotides were designed to replace the wild-type codons with that for alanine (GCT). Mutants of scFvD1.3 were obtained previously (*8*). Prior to expression, all mutations were confirmed by DNA sequencing.

Affinity Measurements. The interaction of soluble scFvD1.3 with immobilized HEL was measured by surface plasmon resonance detection using a BIAcore instrument (Pharmacia Biosensor, Uppsala, Sweden) as described (*8*). The data were analyzed using the BIAevaluation 2.1 software package (Pharmacia). Association constants (K_As) were determined from Scatchard analysis, after correction for nonspecific binding, by measuring the concentration of free reactants and complex at equilibrium. Standard deviations for two or more independent K_A determinations were typically <30%.

Production of HEL Mutant D18A in Yeast. HEL mutant Asp18 → Ala (HEL D18A) was produced using an Invitrogen *Pichia* Expression Kit (San Diego, CA). A cDNA sequence encoding the mutant protein fused with the leader sequence of α mating factor was cloned into plasmid pPic9 as a *Xho*I/*Not*I fragment (*31*). Yeast from a single colony transformed with this plasmid was grown in 25 mL of BMGY medium at 28−30 °C in a shaking incubator at 200−250 rpm. After the culture reached an absorbance of 2.0 at 600 nm, the cells were harvested by centrifuging at 1500*g* for 5 min at room temperature. The pellet was suspended in BMMY medium to an absorbance of 1.0 prior to induction. Methanol was added to the culture to a final concentration of 0.5% (v/v) every 24 h to maintain induction. The culture was harvested by centrifugation after 3 days. The supernatant containing secreted HEL D18A was dialyzed overnight against 0.1 M ammonium acetate, pH 9.0, and loaded on a 3 mL CM-Sepharose Fast Flow column (Pharmacia) previously equilibrated with the same buffer (*32*). The column was washed with 10 vol of buffer; HEL D18A was eluted with 5 column vol of 0.5 M ammonium acetate, pH 9.0. The fractions containing protein were concentrated using a Millipore Centrifugal Filter Device and further purified on a MonoS column as described above for HEL mutants refolded in vitro.

Crystallography. A small molar excess of HEL D18A was added to FvD1.3 prepared as described (*33*) and the mutant complex crystallized by vapor diffusion in hanging drops. The crystallization conditions were similar to those for the wild-type FvD1.3−HEL complex (*34*): 16% (w/v) poly(ethylene glycol) 8000 (Sigma) and 0.1 M potassium phosphate, pH 6.5. The mutant complex crystallized isomorphously with the wild-type in space group *C*2, $a = 128$ Å, $b = 59.8$ Å, $c = 56.3$ Å, and $\beta = 119.3°$. Two sets of

Table 1: Summary of Data Collection and Refinement Statistics

	data set 1	data set 2
data collection		
space group	*C*2	*C*2
unit cell dimensions		
a (Å)	128.07	130.67
b (Å)	59.83	61.21
c (Å)	56.34	57.43
β (deg)	119.27	119.14
X-ray source	CuK_α	synchrotron
maximum resolution (Å)	1.80	1.50
number of observed reflections	85 606	403 840
number of independent reflections	31 162	59 595
R_{merge}[a] (total/	0.059/0.183	0.069/0.301
outer resolution shell)[b]		
completeness (total/	90.1/77.8	90.4/50.6
outer resolution shell;[b] %)		
Refinement		
resolution range (Å)		7.00−1.50
R_{factor}[c] (total/		0.203/0.302
outer resolution shell)[b]		
R_{free}[d] (total/outer resolution shell)[b]		0.251/0.308
number of non-hydrogen protein atoms		2754
number of solvent molecules		486[e]
mean *B*-value		
protein atoms (Å^2)		21.48
solvent atoms (Å^2)		39.27
rms deviations from ideal values		
bond length (Å)		0.012
bond angle (deg)		1.49
dihedral angle (deg)		25.9
improper angle (deg)		1.35

[a] $R_{merge} = \sum|I - \langle I\rangle|/\sum I$. [b] 1.91−1.80 Å for data set 1 and 1.55−1.50 Å for data set 2. [c] $R_{factor} = \sum||F_o| - |F_c||/\sum|F_o|$. [d] 6% of reflections were used for the calculation. [e] Includes one phosphate molecule.

X-ray diffraction data were independently collected for the structure determination (Table 1). Data set 1 was recorded from one complex crystal at 100 K using a Siemens Hi-Star multiwire area detector mounted on a Siemens rotating anode X-ray generator. The crystal was soaked in 16% (w/v) poly(ethylene glycol) 8000, 20% glycerol, and 0.1 potassium phosphate, pH 6.5, prior to flash-cooling in liquid N_2. A total of 85 606 observations were scaled and reduced to 31 162 independent reflections using XENGEN version 2.1 (*35*; Table 1). The data set is 90.1% complete in the resolution range infinity−1.8 Å with R_{merge}= 5.9 and 77.8% complete between 1.9 and 1.8 Å with R_{merge}= 18.3%. The starting structure for the refinement was that of the wild-type complex (*18*) in which HEL Asp18 was replaced with Ala. After rigid body refinement, the temperature factors (*B*) of all atoms were shifted by the grouped *B* factor refinement option of the program X-PLOR (*36*), which simultaneously subtracted approximately 9 Å^2 from the *B* factors of all atoms. This presumably reflects the low temperature at which the mutant data were collected (data for the wild-type complex had been recorded at room temperature). Further refinement consisted of iterative cycles of simulated annealing, positional refinement, and individual *B* factor refinement interspersed with manual model fitting into $F_o - F_c$ and $2F_o - F_c$ electron density maps using O (*37*). During refinement, a higher resolution (1.5 Å) data set became available (data set 2; Table 1). These data were recorded at 100 K using synchrotron radiation (λ = 0.928 Å) at CHESS. A total of 403 840 observations were scaled and reduced to 59 595 independent reflections using DENZO/SCALEPACK (*38*). The data set is 90.4% complete up to 1.5 Å with R_{merge} = 6.9 and 50.6% complete between 1.55 and 1.50 Å with R_{merge} = 30.1%. Refinement was continued using these data. Water molecules were initially placed at positions where the $F_o - F_c$ electron density was greater than 3σ and where reasonable hydrogen bonds were possible. These waters were finally confirmed by R_{omit} profile analysis in which a water molecule is regarded as plausible if the crystallographic R_{factor} calculated without that water is higher than the R_{factor} of the complete structure. One phosphate molecule was placed at a position where a large tetrahedral-shaped electron density feature was observed. The final R_{factor} for the structure is 0.203 for the 56 703 reflections with $F > 3\sigma(F)$ in the range 7.0−1.5 Å with a free-*R* value of 0.251. Two conformations were assigned to 10 side chains. Refinement statistics for the FvD1.3−HEL D18A complex are summarized in Table 1.

RESULTS AND DISCUSSION

Production of HEL Mutants by in Vitro Refolding from Bacterial Inclusion Bodies and by Secretion in Yeast. We used the method of Maeda et al. (*28*) for refolding denatured and reduced HEL in vitro to produce mutants for binding experiments. Although these authors reported refolding yields of up to 90% in the presence of 4 M urea and 3 M sarcosine, our best yields did not exceed 5%. We attribute this difference, at least in part, to the different sources of protein in the two cases. Maeda et al. (*28*) used highly purified commercial HEL to prepare denatured and reduced protein for their refolding experiments, whereas we used HEL isolated from bacterial inclusion bodies and solubilized in urea. We found that refolding yields were critically dependent on the purity of the starting material: inclusion bodies prepared simply by centifugation and washing, even though >90% pure on SDS−PAGE, yielded virtually no active enzyme. Further purification of solubilized HEL polypeptides by sucrose gradient centrifugation and cation-exchange chromatography was required to achieve refolding yields of 2−5%. These additional steps presumably eliminated both protein and nonprotein (e.g., lipid, nucleic acid) contaminants that interfered with refolding, perhaps by causing aggregation of folding intermediates.

While the quantities of HEL mutants that could be conveniently obtained from in vitro refolding (0.1−0.25 mg) were adequate for affinity measurements by BIAcore, they were insufficient for growing crystals of mutant complexes for structural studies. For this purpose, we used the methylotrophic yeast *Pichia pastoris* to express HEL in secreted form (*31*). The advantage of this system is that HEL is expressed and targeted to the supernatant in properly folded form. In addition, *P. pastoris* secretes very low levels of its own proteins, such that the secreted HEL comprises the vast majority of the total protein in the medium, thereby facilitating purification of the secreted product. The yield of purified HEL D18A was 1.0 mg/1 L of yeast culture.

Measurement of Association Constants for the Binding of D1.3 to HEL. A surface plasmon resonance profile for equilibrium binding of scFvD1.3 mutant V_HD54A to immobilized HEL mutant T118A is shown in Figure 1 (panel A). The corresponding Scatchard plot, after correction for nonspecific binding, is also shown (panel B); the apparent K_A, 9.6×10^6 M^{-1}, was calculated as the slope of the straight line. The predicted maximum specific binding, calculated

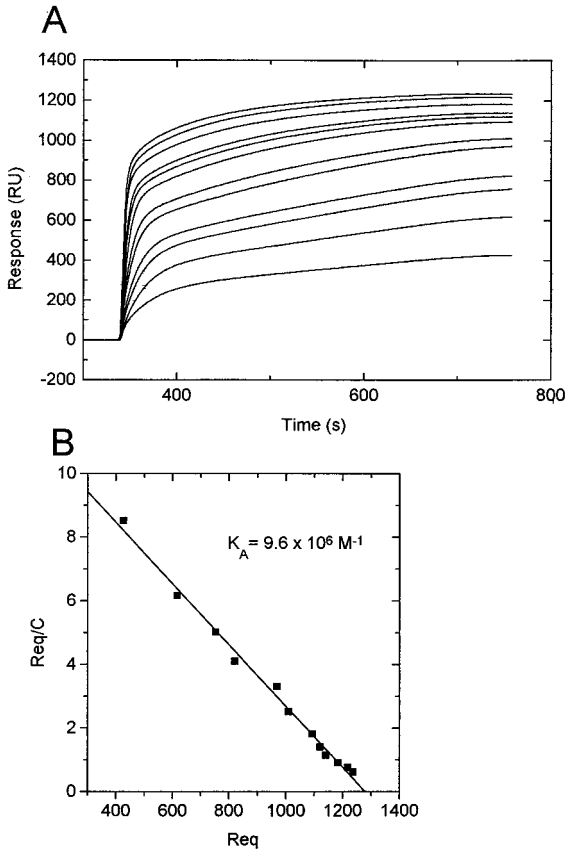

FIGURE 1: (A) Binding of scFv D1.3 D54A to immobilized HEL T118A. The mutant D1.3 was injected at 11 different concentrations ranging from 50 to 2000 nM over a surface to which 830 RU HEL T118A had been coupled. Buffer flow rates were 5 μL/min and report points were taken 7 min after each injection. (B) Scatchard analysis of the binding of scFv D1.3 D54A to HEL T118A derived from the data in (A). The plot is linear with a correlation coefficient of 0.993. The apparent K_A is 9.6 $\times$ 10^6 M^{-1}. The predicted maximum binding capacity (1290 RU) indicated that about 78% of the immobilized HEL molecules are available for binding.

from the *x*-intercept assuming a linear relationship between the mass of bound protein and the measured RU (*39*) indicated that approximately 78% of the immobilized HEL molecules was able to bind scFvD1.3 V_HD54A. The K_As for the interaction of wild-type scFvD1.3 with 12 HEL alanine mutants are shown in Table 2 (section A). Affinity constants have been previously reported for the interaction of wild-type HEL with mutants of D1.3 (*8*). We remeasured each of these K_As in the current study and found them to be in good agreement with the published values. In general, our BIAcore results were extremely reproducible, with errors on K_A consistently less than 30% on repeat measurements of affinity. This translates into errors on $\Delta\Delta G$ and $\Delta\Delta G_{int}$ of less than $\pm$0.2 and $\pm$0.3 kcal/mol, respectively. Thus, the binding of a series of closely related mutant proteins may be compared with a relatively high degree of precision using this method.

Mapping the Energetics of the D1.3−HEL Interface. Alanine scanning mutagenesis of D1.3 residues in contact with HEL in the crystal structure of the FvD1.3−HEL complex had previously shown that the energetics of binding to the antigen are dominated by only 3 of 13 antibody residues tested (*8*). In the present study, we individually mutated 12 of the 13 total nonglycine HEL residues in contact with D1.3 to alanine and measured the affinity of

Table 2: Association Constants and Relative Free-Energy Changes for Single and Double Mutant Complexes[a]

D1.3	HEL	K_A (M^{-1})	$\Delta\Delta G$ (kcal/mol)
WT	WT	$(8.0 \pm 2.4) \times 10^7$	
		Section A	
WT	D18A	$(4.5 \pm 1.4) \times 10^7$	0.3
WT	N19A	$(4.1 \pm 1.2) \times 10^7$	0.3
WT	Y23A	$(4.0 \pm 1.2) \times 10^7$	0.4
WT	S24A	$(1.9 \pm 0.6) \times 10^7$	0.8
WT	K116A	$(2.4 \pm 0.7) \times 10^7$	0.7
WT	T118A	$(2.2 \pm 0.7) \times 10^7$	0.8
WT	D119A	$(1.6 \pm 0.5) \times 10^7$	1.0
WT	V120A	$(1.7 \pm 0.5) \times 10^7$	0.9
WT	Q121A	$(6.2 \pm 1.1) \times 10^5$	2.9
WT	I124A	$(1.0 \pm 0.3) \times 10^7$	1.2
WT	R125A	$(3.6 \pm 1.1) \times 10^6$	1.8
WT	L129A	$(6.0 \pm 1.8) \times 10^7$	0.2
		Section B	
V_LY32A	WT	$(4.4 \pm 1.3) \times 10^6$	1.7
V_LY50A	WT	$(3.3 \pm 1.1) \times 10^7$	0.5
V_LW92A	WT	$(2.8 \pm 0.8) \times 10^5$	3.3
V_HY32A	WT	$(1.2 \pm 0.3) \times 10^7$	1.1
V_HW52A	WT	$(1.7 \pm 0.5) \times 10^7$	0.9
V_HD54A	WT	$(1.5 \pm 0.4) \times 10^7$	1.0
V_HD100A	WT	$(5.6 \pm 0.6) \times 10^5$	2.9
V_HY101A	WT	NB	>4.0
V_HY101F	WT	$(5.5 \pm 1.1) \times 10^6$	1.6
		Section C	
V_LY32A	Q121A	$(1.0 \pm 0.3) \times 10^6$	2.6
V_LY32A	I124A	$(5.9 \pm 1.8) \times 10^5$	2.9
V_LY50A	D18A	$(9.4 \pm 1.0) \times 10^6$	1.3
V_LY50A	D119A	$(1.0 \pm 0.3) \times 10^7$	1.2
V_LW92A	Q121A	$(2.1 \pm 0.6) \times 10^5$	3.5
V_LW92A	I124A	$(1.2 \pm 0.4) \times 10^5$	3.8
V_LW92A	R125A	$(2.6 \pm 0.8) \times 10^5$	3.4
V_LW92A	L129A	$(3.0 \pm 0.9) \times 10^5$	3.3
V_HY32A	K116A	$(5.5 \pm 1.6) \times 10^6$	1.6
V_HW52A	D119A	$(1.8 \pm 0.6) \times 10^6$	2.2
V_HD54A	T118A	$(9.6 \pm 0.3) \times 10^6$	1.2
V_HD100A	S24A	$(2.7 \pm 0.8) \times 10^5$	3.4
V_HY101F	D119A	$(7.9 \pm 2.5) \times 10^5$	2.7
V_HY101F	V120A	$(1.1 \pm 0.3) \times 10^6$	2.5

[a] Affinity measurements were carried out by BIAcore as described in the Materials and Methods. Residue numbering is according to Kabat et al. (*53*). WT refers to wild-type protein. Differences in free-energy changes are calculated as the difference between the ΔGs of the mutant and wild-type reactions ($\Delta\Delta G = \Delta\Delta G_{mutant} - \Delta\Delta G_{wild-type}$). Sections A and B show affinities and $\Delta\Delta G$s for single mutants of HEL and D1.3, respectively. Section C shows values for the double mutants. NB, no binding.

the mutants for wild-type D1.3 (Table 2, section A). Significant decreases in binding ($\Delta\Delta G = 1$ kcal/mol) were only observed for substitutions at four contact positions: Gln121, Ile124, Arg125, and Asp119. The most destabilizing mutation was at position Gln121 ($\Delta\Delta G = 2.9$ kcal/mol). In the wild-type structure, this residue makes two hydrogen bonds to the backbone of V_L complementarity-determining region 3 (CDR3) ($Gln121_{HEL}$ Nϵ2-O V_LPhe91 and $Gln121_{HEL}$ Oϵ1-N V_LSer93) and is nearly completely buried upon complex formation (*18*). Mutations at the remaining eight contact positions (Asp18, Asn19, Tyr23, Ser24, Lys116, Thr118, Val120, and Leu129) had little or no effect ($\Delta\Delta G < 1$ kcal/mol). Therefore, for both the D1.3 and HEL sides of this interface, only small subsets of the total contacting residues appear to account for a large portion of the binding energy. This result is similar to findings in the case of human growth homone binding to its receptor (*13*, *14*), but differs from the interaction of D1.3 with the anti-D1.3 antibody E5.2

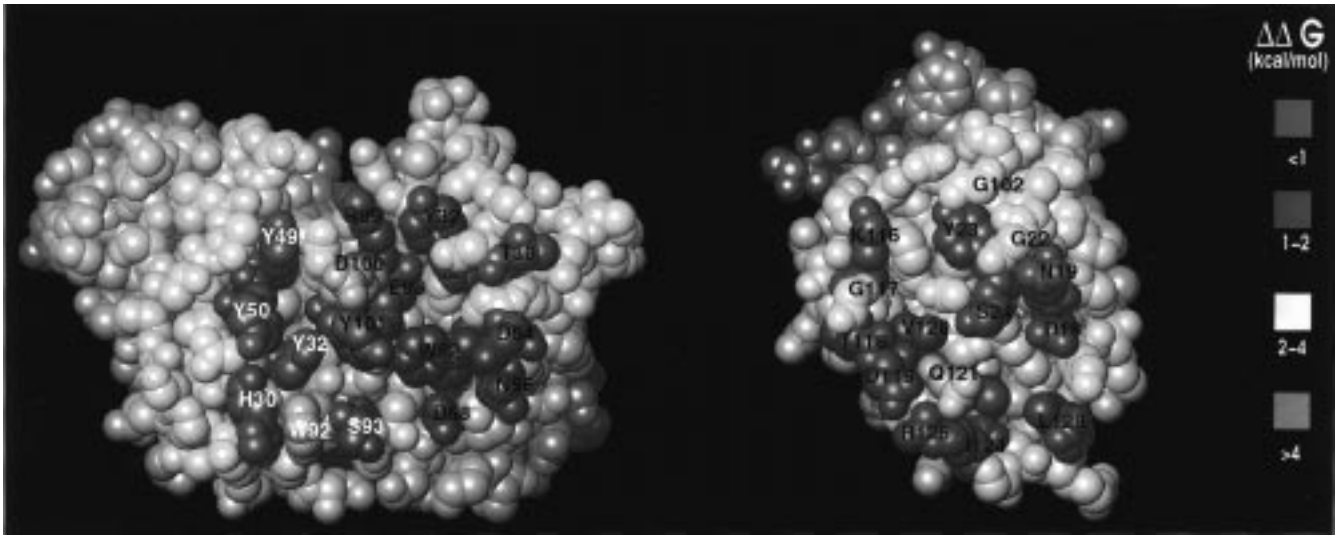

FIGURE 2: Space-filling model of the surface of D1.3 (left) in contact with HEL and of the surface of HEL (right) in contact with D1.3. The two proteins are oriented such that they may be docked by folding the page along a vertical axis between the components. Residues are color-coded according to the loss of binding free energy upon alanine substitution: red, >4 kcal/mol; yellow, 2−4 kcal/mol; green, 1−2 kcal/mol; blue, <1 kcal/mol. V_L residues are labeled in white and V_H residues in black. Glycine residues on HEL in contact with D1.3 are labeled at their α-carbons.

in which nearly all D1.3 and E5.2 residues in contact in the crystal structure play a significant role in complex stabilization (*9*). It also differs from the interaction of the T cell receptor β chain with the bacterial superantigen staphylococcal enterotoxin C, where 8 of 11 superantigen residues in contact with the β chain were shown to be energetically important to binding (*10*). Thus, at least on the basis of this limited number of examples, it appears that protein−protein interfaces fall into one of two general categories: (i) ones in which a small subset of contact residues on both protein surfaces dominate the energetics of the association reaction or (ii) ones in which most contact residues on both proteins mediate productive binding. However, it cannot be excluded that, in other protein−protein interfaces, a surface in which only a few residues significantly contribute to binding may juxtapose one in which the majority of residues do.

Figure 2 shows the residues of D1.3 and HEL important in complex stabilization mapped onto the three-dimensional structure of each protein. The residues of HEL most important for binding D1.3 (Asp119, Gln121, Ile124, and Arg125) form a contiguous patch located at the periphery of the surface contacted by the antibody. In the three-dimensional structure of the complex, Gln121 penetrates a hydrophobic pocket where it is surrounded by the aromatic side chains of V_LTyr32, V_LTrp92, and V_HTyr101 (*18*). A comparison of the two surfaces in Figure 2 reveals that hot spot residues on the D1.3 side of the interface generally correspond to hot spot positions on the HEL side. For example, HEL hot spot residues Gln121 ($\Delta\Delta G = 2.9$ kcal/mol) and Arg125 (1.8 kcal/mol) contact D1.3 hot spot residue V_LTrp92 (3.3 kcal/mol); in addition, $Gln121_{HEL}$ contacts V_L-Tyr32 (1.7 kcal/mol) and V_HTyr101 (>4.0 kcal/mol). Similarly, functionally less important D1.3 and HEL residues tend to be juxtaposed in the antigen−antibody interface: $Asp18_{HEL}$ ($\Delta\Delta G = 0.3$ kcal/mol) and Thr118 (0.8 kcal/mol) interact with D1.3 V_LTyr50 (0.5 kcal/mol) and V_HTrp52 (0.9 kcal/mol), respectively. A significant exception to this complementarity is $Ile124_{HEL}$, which is more than 4 Å away from any D1.3 residue, yet whose replacement by alanine results in a decrease in binding free energy of 1.2 kcal/mol. However, since the Ile124 side chain is partially buried in HEL, this may be an indirect effect due to structural perturbations in the antigen propogating from the mutation to neighboring D1.3-contacting residues, particularly Arg125. Similar considerations probably apply to V_HGlu98 ($\Delta\Delta G =$ 1.1 kcal/mol), which is mostly buried in the D1.3 combining site but which contacts V_HAsp100 and V_HTyr101. In several cases, the side chains of D1.3 hot spot residues interact with HEL main-chain atoms (e.g., V_HAsp100 Oγ1-N $Ser24_{HEL}$), such that the relative contribution of the HEL residue cannot be assessed by simple alanine substitution. Overall, however, our results are in agreement with findings in the growth hormone-growth hormone receptor (*14*) and D1.3−E5.2 (*9*) systems that energetically critical residues on one protein match those on its partner in the corresponding complex. As in the case of these two other complexes, the buried surface area of individual HEL residues upon complex formation does not correlate well with their relative importance in binding D1.3 (data not shown).

A modeling analysis of the D1.3−HEL interface by Covell and Wallqvist (*40*) based on pairwise surface preferences predicted that the largest changes in binding free energy should arise from mutation of HEL residues Asn19 and Gln121. Their calculations further suggested that three glycine residues at HEL positions 22, 102, and 117, all of which make hydrogen bonds to D1.3, also contribute significantly to the binding. While the energetic contribution of glycine residues cannot be evaluated by alanine scanning, we did indeed find Gln121 to be functionally the most important residue among those tested (Table 2, section A). However, contrary to prediction, we also found $Asn19_{HEL}$ to make essentially no net contribution to complex stabilization ($\Delta\Delta G = 0.3$ kcal/mol). This is surprising since Asn19 makes one short hydrogen bond (V_LThr53 Oγ1-Nδ2 $Asn19_{HEL}$; 2.8 Å), as well as a number of van der Waals contacts, with D1.3 in the crystal structure of the complex (*18*).

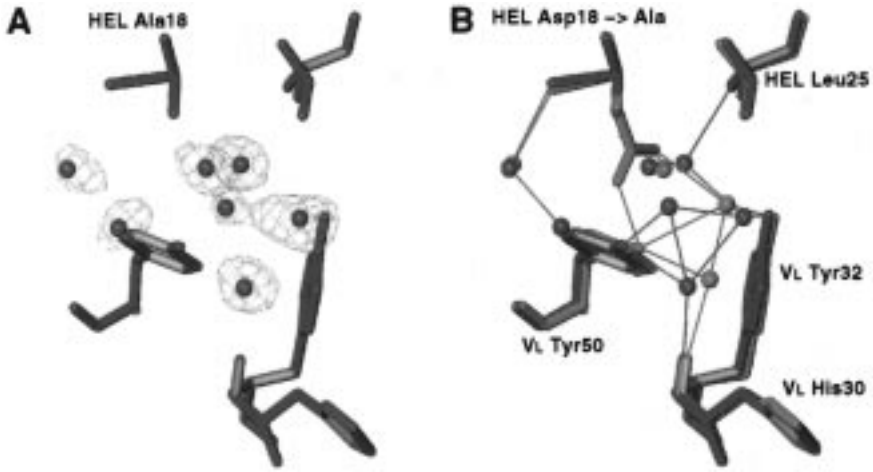

FIGURE 3: (A) Omit map of seven interface water molecules (spheres) in the vicinity of HEL Ala18 (labeled) in the FvD1.3 HEL D18A mutant complex. Contours are at 2σ. (B) Superposition of the FvD1.3 HEL D18A mutant complex (green) onto the wild-type structure (red). The view is the same as in panel A. Hydrogen bonds are drawn as thin lines.

Structural Basis for the Accommodation of a Potentially Disruptive Mutation in the D1.3−HEL Interface. The results described above demonstrate that the D1.3−HEL interface is remarkably tolerant to mutations which, on the basis of the three-dimensional structure of the wild-type complex, might be expected to have pronounced effects on affinity. For example, truncation of HEL residue Asp18 to alanine should result in the loss of a direct hydrogen bond to the side chain of D1.3 V_LTyr50 ($Asp18_{HEL}$ Oδ2-Oη D1.3 V_L-Tyr50), as well as the loss of seven van der Waals contacts to this residue ($Asp18_{HEL}$ Cγ-Cϵ2 V_LTyr50, $Asp18_{HEL}$ Cγ-Cζ V_LTyr50, $Asp18_{HEL}$ Cγ-Oη V_LTyr50, $Asp18_{HEL}$ Oδ2-Cϵ2 V_LTyr50, $Asp18_{HEL}$ Oδ2-Cζ V_LTyr50, $Asp18_{HEL}$ Oδ1-Cζ V_LTyr50, and $Asp18_{HEL}$ Oδ1-Oη V_LTyr50). Nevertheless, the affinity of HEL D18A for D1.3 (4.5×10^7 M^{-1}) is nearly identical to that of the wild-type (8.0×10^7 M^{-1}), corresponding to a $\Delta\Delta G$ of only 0.3 kcal/mol (Table 2, section A). To understand how this mutation is nearly completely accommodated in the D1.3−HEL interface, we determined the crystal structure of the FvD1.3−HEL D18A complex at 1.5 Å resolution. To our knowledge, this represents the highest resolution structure yet reported for an antigen−antibody complex involving a protein antigen. An omit map in the region of the mutation is shown in Figure 3a. The rms difference in α-carbon positions between mutant and wild-type structures is only 0.45 Å, which is comparable to an average error in atomic positions of 0.2 Å estimated using Luzzati plots (*41*). This indicates that the mutation does not significantly affect the overall structure of the complex. Conformational changes in the proteins at the site of the mutation are also small (Figure 3b).

The major difference in the structure of the FvD1.3−HEL D18A complex is a rearrangement of solvent such that three additional water molecules are stably incorporated in the interface at the site of the mutation (Figure 4a). These bound waters (designated WATa, WATb, and WATc) form several hydrogen bonds with protein atoms and with other water molecules, some of which mimic hydrogen bonds made by HEL Asp18. In the wild-type structure (Figure 4b), one of the carbonyl oxygens of HEL Asp18 forms two hydrogen bonds with WAT1 and WAT2; the latter is in turn hydrogen bonded to the hydroxy group of V_LTyr32. In the mutant, WATa serves as a substitute for Asp18 by partially occupying some of the volume taken up by the side chain of this residue and by making hydrogen bonds with WAT1 and WAT2, thereby preserving the interface water network. In addition, WATa forms a hydrogen bond with the main chain-nitrogen of HEL Leu25, which further anchors it in the interface. The other carbonyl oxygen of HEL Asp18 forms a direct hydrogen bond with the hydroxy group of V_LTyr50 in the wild-type structure (Figure 4b). In the mutant, V_L-Tyr50 makes hydrogen bonds with WATb and WATc which, like WATa, are positioned to help fill the cavity created by the mutation and form part of the rearranged solvent network bridging antigen and antibody. Thus, the loss of complementarity in the D1.3−HEL interface resulting from replacement of HEL Asp18 by alanine is compensated by the stable inclusion of additional water molecules and by local rearrangements in solvent structure rather than by adjustments in the conformation of the protein. Similar mechanisms may explain the tolerance of the D1.3−HEL interface to mutations at other solvent-accessible sites on the antigen, such as HEL Ser24 and Lys116, which also make multiple contacts with D1.3.

We had previously observed solvent rearrangements, including the incorporation of additional interface waters, in X-ray crystallographic studies of three site-directed mutants of FvD1.3 complexed with wild-type HEL: V_L-Y50S, V_HY32A, and V_LW92D (*7, 33*). In the FvD1.3 V_L-Y50S−HEL complex (Figure 4c), for example, two additional waters (WATd and WATe) occupy some of the volume taken up by the V_LTyr50 side chain in the wild-type structure. In these cases, however, the mutations were only partially compensated by the solvent rearrangements, since the V_LY50S, V_HY32A, and V_LW92D mutant fragments bound HEL with 10-, 4-, and 1000-fold lower affinities, respectively, than the original antibody. Thus, there appears to be a wide range in the extent to which solvent rearrangements in a protein−protein interface can accommodate mutations, which probably depends on the nature of the local environment. In this respect, it is interesting to note that V_LTyr50 and HEL Asp18 are juxtaposed in the complex structure (Figure 4b). This suggests that these two residues define a site in the interface that, perhaps because of its peripheral location (Figure 2), is particularly suited for the

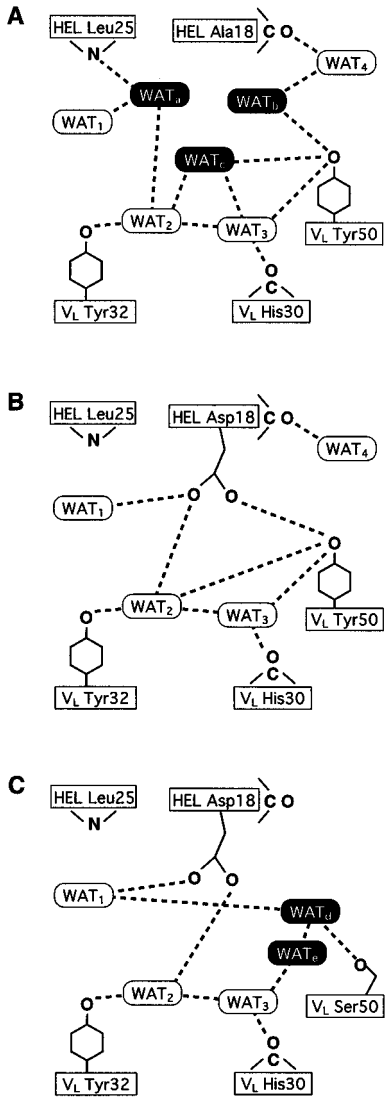

FIGURE 4: (A) Schematic representation of the FvD1.3−HEL D18A complex in the vicinity of the mutation. (B) Schematic showing the same region in the wild-type FvD1.3−HEL complex (*18*). (C) Schematic of the FvD1.3 V_LS50A−HEL mutant complex (*33*). Water molecules present in all three structures are labeled WAT1, WAT2, and WAT3; WAT4 is present in only the FvD1.3−HEL D18A and wild-type complexes. WATa, WATb, and WATc are additional waters in the FvD1.3−HEL D18A interface; WATd and WATe are additional waters in the FvD1.3 V_LS50A−HEL interface. Hydrogen bonds are drawn as dotted black lines.

stable incorporation of new waters to occupy cavities or channels created by side-chain truncations.

Analysis of the D1.3−HEL Interface Using Double Mutant Cycles. As pointed out by Fersht (*42*), comparing the binding of a wild-type protein with that of a mutant in which a side chain has been truncated gives an apparent binding energy which is generally different from the incremental binding energy attributable to that side chain. In principle, the method of double mutant cycles overcomes most of the limitations of single mutant experiments and makes it possible to estimate the effective interaction energy between specific residues in each member of a protein−protein complex independently of all interactions except those between the residues mutated in the cycle (*21*−*23*). Thus, FvD1.3 residue A and HEL residue B were mutated (i.e., A → A′, B → B′) separately and together to construct the following cycle:

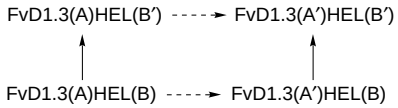

The coupling, or interaction, energy between residues A and B ($\Delta\Delta G_{int}$) is then given by

$$\Delta\Delta G_{int} = -\Delta\Delta G_{AB\rightarrow A'B'} + \Delta\Delta G_{AB\rightarrow A'B} + \Delta\Delta G_{AB\rightarrow AB'} \quad (1)$$

If $\Delta\Delta G_{int}$ equals zero, the effects of the two mutations are independent of each other and the two residues are not coupled. A $\Delta\Delta G_{int}$ other than zero indicates that residues A and B are coupled, either directly or indirectly, since the change in free energy for the association of the double mutant complex is different from the sum of those for the two single mutant complexes. The coupling energy between two residues is defined thermodynamically and makes no assumptions about the underlying structural mechanisms nor does it necessarily imply a proximity correlation (*22*).

Double mutant cycles were constructed for 14 amino acid pairs in the D1.3−HEL interface in order to map the interaction energies at the contact surfaces between these two proteins (Table 2, section C). Of the 14 pairs tested, 10 have interacting side chains as judged from the crystal structure, 2 do not form direct contacts but are in proximity (4 Å), and 2 are far apart (6−15 Å). Coupling energies were calculated according to eq 1 and are given in Table 3. Surprisingly, only 3 of the 10 residue pairs in direct contact in the crystal structure show coupling energies of greater than 1.0 kcal/mol: V_LTyr32-Gln121$_{HEL}$ (2.0 kcal/mol), V_LTrp92-Gln121$_{HEL}$ (2.7 kcal/mol), and V_LTrp92-Arg125$_{HEL}$ (1.7 kcal/mol). Indeed, with the exception of the residue pair V_HAsp54-Thr118$_{HEL}$ ($\Delta\Delta G_{int}$ = 0.6 kcal/mol), none of the remaining seven residue pairs have coupling energies exceeding the estimated experimental error of ± 0.3 kcal/mol: V_LTyr50-Asp18$_{HEL}$ (−0.4 kcal/mol), V_HTyr32-Lys116$_{HEL}$ (0.2 kcal/mol), V_HTrp52-Asp119$_{HEL}$ (−0.3 kcal/mol), V_HAsp100-Ser24$_{HEL}$ (0.3 kcal/mol), V_HTyr101-Asp119$_{HEL}$ (−0.1 kcal/mol), and V_HTyr101-Val120$_{HEL}$ (0.0 kcal/mol). In fact, in terms of their coupling energies, these residue pairs are indistinguishable from the four pairs that do not form direct contacts: V_LTyr32-Ile124$_{HEL}$ ($\Delta\Delta G_{int}$ = 0.0 kcal/mol), V_LTyr50-Asp119$_{HEL}$ (0.3 kcal/mol), V_LTrp92-Ile124$_{HEL}$ (0.7 kcal/mol), and V_LTrp92-Leu129$_{HEL}$ (0.2 kcal/mol). Therefore, the simple fact that two residues make direct contacts in a protein−protein interface does not necessarily imply that there exists a net productive interaction between them. In fact, the majority of such contacts may be energetically neutral, as in the present case.

These findings are in marked contrast to those for the D1.3−E5.2 (*9*) and barnase−barstar (*43*) complexes in which nearly all residues within 4 Å of each other showed significant coupling (>1.0 kcal/mol). In the D1.3−E5.2 and barnase−barstar interfaces, the relative strengths of coupling energies were, in most cases, broadly consistent with expectations based on the crystal structures. For example, the highest coupling energy (4.3 kcal/mol) in the D1.3−E5.2 complex was measured for a charged-neutral pair forming a buried hydrogen bond, while side chains interacting through solvated hydrogen bonds had lower coupling energies (1.3−1.7 kcal/mol) and solvent-mediated hydrogen bonds were

Table 3: Coupling Energies between the Indicated Amino Acid Pairs in the FvD1.3−HEL Complex as Measured by Double Mutant Cycles[a]

D1.3	HEL	$\Delta\Delta G_{int}$ (kcal/mol)	number and type of side chain−side chain interactions lost in double mutants
V_LY32	Q121	2.0	1 hydrogen bond
	I124	0.0	no direct contacts (4.1 Å apart)
V_LY50	D18	−0.4	1 hydrogen bond (solvent exposed)
			7 van der Waals contacts
	D119	0.3	no direct contacts (14 Å apart)
V_LW92	Q121	2.7	3 van der Waals contacts
	R125	1.7	3 van der Waals contacts
	I124	0.7	no direct contacts (4.1 Å apart)
	L129	0.2	no direct contacts (6.5 Å apart)
V_HY32	K116	0.2	1 van der Waals contact
			1 long hydrogen bond*
V_HW52	D119	−0.3	3 van der Waals contacts
V_HD54	T118	0.6	1 van der Waals contact
V_HD100	S24	0.3	1 hydrogen bond (in water channel)
			1 van der Waals contact
V_HY101	D119	−0.1	1 hydrogen bond (partially buried)
			1 van der Waals contact
	V120	0.0	1 van der Waals contact

[a] Coupling energies are defined as $\Delta\Delta G_{int} = \Delta\Delta G_{AB\rightarrow A'B} + \Delta\Delta G_{AB\rightarrow AB'} - \Delta\Delta G_{AB\rightarrow A'B'}$, where A and B represent wild-type and HEL residues, respectively, and A′ and B′ represent the mutated residues. All cycles were alanine truncations except the cycle with V_HY101 which involved a phenylalanine substitution. Intermolecular contacts were defined by atomic pair distances (Å) less than or equal to the following: C−C, 4.1; C−N, 3.8; C−O, 3.7; N−N, 3.4; N−O, 3.4; O−O, 3.3. The one exception is the hydrogen bond labeled with an asterisk (*) between D1.3 V_HY32 and HEL K116 with a N−O bond distance of 3.5 Å.

energetically neutral (*9*). However, with one exception (see below), none of the hydrogen bonds we examined in the D1.3−HEL interface make significant net contributions to complex stabilization (Table 3). These include hydrogen bonds which, on the basis of donor−acceptor distance and relative orientation of the interacting groups, would be predicted to be strong, as well as ones expected to be weak. For example, V_HTyr101 is situated near the center of the D1.3−HEL interface and makes a short (2.7 Å) hydrogen bond with good geometry to HEL residue Asp119 (V_HTyr101 Oη-Oγ1 Asp119$_{HEL}$); in addition, this hydrogen bond involves a charged-neutral pair and is buried in the interface. We therefore expected a $\Delta\Delta G_{int}$ of 3−4 kcal/mol, based on measurements in other systems (*9*, *44*−*46*). However, the observed $\Delta\Delta G_{int}$ for the V_HTyr101-Asp119$_{HEL}$ residue pair is in fact −0.1 kcal/mol, which is zero within experimental error (Table 3). Similarly, V_LTyr50 and V_HAsp100 make "strong" hydrogen bonds with HEL Asp18 and Ser24, respectively: V_LTyr50 Oη-Oγ2 Asp18$_{HEL}$ (2.7 Å) and V_H-Asp100 Oδ2-Oγ Ser24$_{HEL}$ (2.8 Å). Although these two bonds are solvated and might therefore be expected to be weaker than the buried V_HTyr101 Oη-Oγ1 Asp119$_{HEL}$ hydrogen bond, we had previously measured $\Delta\Delta G_{int}$ values of about 1.5 kcal/mol for residue pairs making similar bonds in the D1.3−E5.2 interface (*9*). Nevertheless, there is no apparent interaction between the hydrogen-bonded V_LTyr50-Asp18$_{HEL}$ and V_HAsp100-Ser24$_{HEL}$ residue pairs in the D1.3−HEL complex (Table 3). Finally, V_HTyr32 makes a long (3.5 Å), solvent-exposed hydrogen bond to HEL Lys116 (V_HTyr32 Oη-Nζ Lys116$_{HEL}$). No coupling was found between these residues ($\Delta\Delta G_{int} = -0.1$), but this bond was expected to be weak.

The only hydrogen-bonded residues in this protein−protein interface to show significant coupling are Gln121$_{HEL}$ and V_L-Tyr32 ($\Delta\Delta G_{int} = 2.0$ kcal/mol). This interaction consists of a hydrogen bond between the Nϵ2 group of Gln121 acting as a hydrogen bond donor and the center of the phenyl ring of V_LTyr32 acting as a hydrogen bond acceptor. Levitt and Perutz (*47*) calculated that hydrogen bonds with aromatic rings as proton acceptors should contribute approximately 3 kcal/mol of stabilizing free energy to molecular associations, which is in good agreement with our measured value of 2.0 kcal/mol.

The reasons for the observed differences between actual and expected coupling energies for most of the hydrogen-bonded residue pairs we examined are probably best understood in terms of an analysis of the theory of double mutant cycles by Serrano et al. (*48*). If A and B are two hydrogen-bonded residues and the mutations A → A′ and B → B′ are nondisruptive (i.e., neither A nor any other protein residue moves upon mutating B and vice versa), the coupling energy between A and B is given by

$$\Delta\Delta G_{int} = G_{A/B} - \Delta G_{A/solv} - \Delta G_{B/solv} \qquad (2)$$

where $\Delta G_{A/solv}$ is the solvation energy of A, $\Delta G_{B/solv}$ is the solvation energy of B, and $G_{A/B}$ is energy of the hydrogen bond between A and B. If mutation of A allows water to bind to B, and vice versa, $\Delta G_{A/solv}$ and $\Delta G_{B/solv}$ are the energies of the hydrogen bonds with water. Equation 2 then measures the free energy change for the exchange reaction $A-H_2O + H_2O-B \leftrightarrow A-B + H_2O-H_2O$ in which A and B exchange their interactions with water to interact with each other. If there is no access of water on mutation of A or B, $\Delta G_{A/solv} + \Delta G_{B/solv}$ is zero and $\Delta\Delta G_{int} = G_{A/B}$. For the interaction of V_LTyr50 with HEL Asp18 ($\Delta\Delta G_{int} = -0.4$ kcal/mol), high-resolution X-ray crystallographic analysis of the single mutant complexes has clearly shown that the hydrogen-bonding potentials of the V_LTyr50 and Asp18$_{HEL}$ side chains are satisfied in the mutants and that the mutations are nondisruptive. For the FvD1.3 V_LY50S−HEL complex (*33*), both carboxylate atoms of Asp18$_{HEL}$ are hydrogen bonded to interface solvent molecules (Figure 4c), as is the hydroxy group of V_LTyr50 in the FvD1.3−HEL D18A complex (Figure 4a). It is therefore likely that, at least in this case, $\Delta\Delta G_{int}$ is a measure of the free-energy change of the exchange reaction, rather than of the intrinsic energy of the V_LTyr50 Oη-Oδ2 Asp18$_{HEL}$ hydrogen bond. Since this $\Delta\Delta G_{int}$ is effectively zero, the strength of this particular protein−protein hydrogen bond is comparable to that of the water−protein hydrogen bonds it replaces and the bond makes no net contribution to complex stabilization. The observed lack of coupling between other hydrogen-bonded residue pairs in the D1.3−HEL interface may be similarly explained. However, this does not account for the finding that hydrogen-bonded residue pairs in the D1.3−E5.2 interface showed coupling energies of 1−4 kcal/mol (*9*). One possibility is that there is no access (or restricted access) of solvent on mutation of residues A or B in the D1.3−E5.2 complex such that $\Delta\Delta G_{int}$ more closely reflects $G_{A/B}$. This is unlikely in the case of solvated hydrogen bonds, but probably applies to buried ones. Alternatively, hydrogen bond strengths may be highly dependent on local environment (for example, on the dielectric constant at the site of

mutation), such that even bonds of similar lengths and geometry may possess very different energies. X-ray crystallographic studies of D1.3−E5.2 mutant complexes will be required to distinguish between these possibilities for individual hydrogen-bonded residue pairs. Regardless of the physical interpretation of our $\Delta\Delta G_{int}$ measurements in terms of the actual strength of individual bonds in the D1.3−HEL and D1.3−E5.2 interfaces, however, the fact remains that a $\Delta\Delta G_{int}$ equal to zero for any two target residues indicates that there is no net interaction between them. Therefore, the results from double mutant cycles confirm our conclusion from single mutant experiments that most D1.3−HEL contacts are energetically neutral and do not contribute to complex stabilization.

The interaction of $Gln121_{HEL}$ with V_LTrp92 had the largest coupling energy ($\Delta\Delta G_{int}$ = 2.7 kcal/mol). Since this interaction involves only three van der Waals contacts, whose strength has been estimated at about 0.5 kcal/mol per contact (*7*, *9*), this implies that this $\Delta\Delta G_{int}$ almost certainly includes a significant contribution from the hydrophobic effect arising from burial of the tryptophan side chain. Similar considerations may apply to the interaction of V_LTrp92 with $Arg125_{HEL}$ ($\Delta\Delta G_{int}$ = 1.7 kcal/mol).

Of the four residue pairs not involved in direct contacts in the crystal structure (V_LTyr32-$Ile124_{HEL}$, 4.1 Å; V_LTyr50-$Asp119_{HEL}$, 14 Å; V_LTrp92-$Ile124_{HEL}$, 4.1 Å; and V_LTrp92-$Leu129_{HEL}$, 6.5 Å), only V_LTrp92 and $Ile124_{HEL}$ showed significant coupling (0.7 kcal/mol). However, this may result from secondary interactions through a third residue, $Arg125_{HEL}$, which contacts both V_LTrp92 and $Ile124_{HEL}$. We do not find examples of long-range interactions as in the D1.3−E5.2 (*9*), barnase−barstar (*43*), and hemoglobin dimer−dimer (*49*) interfaces, although a more extensive survey of noncontacting residues would likely reveal these.

CONCLUSIONS

We have shown by alanine scanning mutagenesis of HEL residues in contact with D1.3 that the energetics of binding to the antibody are dominated by only 2 of 12 antigen residues tested ($\Delta\Delta G$ > 1.5 kcal/mol). A similar observation was made for the D1.3 side of the interface, where only 3 of 13 antibody residues were found to play a significant role in ligand binding (*8*). Thus, a small subset of contact residues on each of these proteins dominates the energetics of the association reaction. This is in contrast to the D1.3−E5.2 interface in which most contact residues on both proteins mediate productive binding (*9*). In both interfaces, however, energetically important residues tend to be juxtaposed. These results demonstrate that the D1.3−HEL interface, unlike the D1.3−E5.2 interface, is very tolerant to mutations. The crystal structure at 1.5 Å resolution of the complex between D1.3 and HEL D18A reveals how a potentially destabilizing mutation that results in the loss of a hydrogen bond and of a number of van der Waals contacts is accommodated in the interface ($\Delta\Delta G$ = 0.3 kcal/mol). In the mutant complex, three new water molecules are incorporated in the interface where they occupy a cavity created by the mutation and form part of a rearranged solvent network linking antigen and antibody. These bound waters compensate the loss of complementarity at the site of the mutation and satisfy the hydrogen-bonding potential of neighboring residues. No significant adjustments in protein structure are observed. Similar mechanisms probably explain the ability of the D1.3−HEL interface to accommodate mutations at other solvent-accessible sites.

The use of double mutant cycles has enabled us to quantitate the interaction between specific amino acid pairs in the D1.3−HEL complex. Surprisingly, only 3 of 10 residue pairs in direct contact in the crystal structure showed significant coupling, in contrast to other protein−protein interfaces in which nearly all residues within 4 Å of each other displayed coupling energies exceeding 1.0 kcal/mol (*9*, *43*). With the exception of the two residues forming a hydrogen bond with a phenyl ring as proton acceptor, none of the other four hydrogen-bonded residue pairs we examined make a net contribution to stabilizing the D1.3−HEL complex, even though they involve hydrogen bonds expected to be strong. We attribute these results to the accessibility of the mutation sites to water, such that the mutated residues exchange their interaction with each other for interactions with water. This implies that the strength of these particular protein−protein hydrogen bonds is comparable to that of the protein−water hydrogen bonds they replace. Therefore, the fact that two residues form direct contacts in a protein−protein interface is not necessarily an indication that there exists a productive interaction between them. Instead, the majority of such interactions may be energetically neutral, as in the D1.3−HEL complex. These results demonstrate that considerable caution should be exercised when attempting to estimate the strengths of specific interactions in a protein−protein interface on the basis of three-dimensional structures alone. Although recent computational methods for predicting the strengths of these interactions appear promising (*40*, *50*−*52*), information on the relative contribution of individual residues to complex stabilization can only be reliably obtained at the present time through actual affinity measurements of site-directed mutants of the interacting species.

REFERENCES

1. Janin, J., and Chothia, C. (1990) *J. Biol. Chem. 265*, 16027−16030.
2. Wilson, I. A., and Stanfield, R. L. (1993) *Curr. Opin. Struct. Biol. 3*, 113−118.
3. Braden, B. C., and Poljak, R. J. (1995) *FASEB J. 9*, 9−16 (1995).
4. Davies, D. R., and Cohen, G. H. (1996) *Proc. Natl. Acad. Sci. U.S.A. 93*, 7−12.
5. Tulip, W. R., Varghese, J. N., Laver, W. G., Webster, R. G., and Colman, P. M. (1992) *J. Mol. Biol. 227*, 122−148.
6. Tulip, W. R., Varghese, J. N., Webster, R. G., Laver, W. G., and Colman, P. M. (1992) *J. Mol. Biol. 227*, 149−159.
7. Ysern, X., Fields, B. A., Bhat, T. N., Goldbaum, F. A., Dall'Acqua, W., Schwartz, F. P., Poljak, R. J., and Mariuzza, R. A. (1994) *J. Mol. Biol. 238*, 496−500.
8. Dall'Acqua, W., Goldman, E. R., Eisenstein, E., and Mariuzza, R. A. (1996) *Biochemistry 35*, 9667−9676.
9. Goldman, E. R., Dall'Acqua, W, Braden, B. C., and Mariuzza, R. A. (1997) *Biochemistry 36*, 49−56.
10. Leder, L., Llera, A., Lavoie, P. M., Lebedeva, M. I., Li, H., Sékaly, R. P., Bohach, G. A., Gahr, P. J., Schlievert, P. M., Karjalainen, K., and Mariuzza, R. A. (1998) *J. Exp. Med. 187*, 823−833.
11. Novotny, J., Bruccoleri, R. E., and Saul, F. A. (1989) *Biochemistry 28*, 4735−4749.
12. Kelley, R. F., and O'Connell, M. P. (1993) *Biochemistry 32*, 6828−6835.

13. Cunningham, B. C., and Wells, J. A. (1993) *J. Mol. Biol. 234*, 554−563.
14. Clackson, T., and Wells, J. A. (1995) *Science 267*, 383−386.
15. Kam-Morgan, L. N. W., Smith-Gill, S. J., Taylor, M. G., Zhang, E., Wilson, A. C., and Kirsch, J. F. (1993) *Proc. Natl. Acad. Sci. U.S.A. 90*, 3958−3962.
16. Malby, R. L., Tulip, W. R., Harley, V. R., McKimm-Breschkin, J. L., Laver, W. G., Webster, R. G., and Colman, P. M. (1994) *Structure 2*, 733−746.
17. Chacko, S., Silverton, E. W., Kam-Morgan, L., Smith-Gill, S. J., Cohen, G., and Davies, D. R. (1995) *J. Mol. Biol. 245*, 261−274.
18. Bhat, T. N., Bentley, G. A., Boulot, G., Greene, M. I., Tello, D., Dall'Acqua, W., Souchon, H., Schwarz, F. P., Mariuzza, R. A., and Poljak, R. J. (1994) *Proc. Natl. Acad. Sci. U.S.A. 91*, 1089−1093.
19. Fields, B. A., Goldbaum, F. A., Ysern, X., Poljak, R. J., and Mariuzza, R. A. (1995) *Nature 374*, 739−742.
20. Braden, B. C., Fields, B. A., Ysern, X, Dall'Acqua, W, Goldbaum, F. A., Poljak, R. J., and Mariuzza, R. A. (1996) *J. Mol. Biol. 264*, 137−151.
21. Carter, P. J., Winter. G., Wilkinson, A. J., and Fersht, A. R. (1984) *Cell 38*, 835−840.
22. Ackers, G. K., and Smith, F. R. (1985) *Annu. Rev. Biochem. 54*, 597−629.
23. Horovitz, A. (1987) *J. Mol. Biol. 196*, 733−735.
24. McCafferty, J., Griffiths, A. D., Winter, G., and Chiswell, D. J. (1990) *Nature 348*, 552−554.
25. van der Merwe, P. A., Barclay, A. N., Mason, D. W., Davies, E. A., Morgan, B. P., Tone, M., Krishnam, A. K. C., Ianelli, C., and Davis, S. J. (1994) *Biochemistry 33*, 10149−10160.
26. Sanger, F., Nicklen, S., and Coulson, A. R. (1977) *Proc. Natl. Acad. Sci. U.S.A. 74*, 5463−5467.
27. Goldberg, M. E., Rudolph, R., and Jaenicke, R. (1991) *Biochemistry 30*, 2790−2797.
28. Maeda, Y., Yamada, H., Ueda, T., and Imoto, T. (1996) *Protein Eng. 9*, 461−465.
29. Charlemagne, D., and Jolles, P. (1970) *C. R. Acad. Sci. Paris*, 2721−2723.
30. Kunkel, T. A., Roberts, J. D., and Zakour, R. A. (1987) *Methods Enzymol. 154*, 367−382.
31. Li, Y., Grivel, J.-C., Visiwanathan, M., Srinivasan, M., and Smith-Gill, S. J. (1997) *FASEB J. 11*, A1043.
32. Malcolm, B. A., Rosenberg, S., Corey, M. J., Allen, J. S., de Baetselier, A., and Kirsch, J. F. (1989) *Proc. Natl. Acad. Sci. U.S.A. 86*, 133−137.
33. Fields, B. A., Goldbaum, F. A., Dall'Acqua, W, Malchiodi, E. L., Cauerhff, A., Schwarz, F. P., Ysern, X, Poljak, R. J., and Mariuzza, R. A. (1996) *Biochemistry 35*, 15494−15503.
34. Boulot, G., Eisele, J.-L., Bentley, G. A., Bhat, T. N., Ward, E. S., Winter, G., and Poljak, R. J. (1990) *J. Mol. Biol. 213*, 617−619.
35. Howard, A. J., Gilliland, G. L., Finzel, B. C., Poulos, T. L., Ohlendorf, D. H., and Salemme, F. R. (1987) *J. Appl. Crystallogr. 20*, 383−387.
36. Brunger, A. T. (1992) *X-PLOR Version 3.1. A System for X-ray Crystallography and NMR*, Yale University Press, New Haven and London.
37. Jones, T. A., Zou, J. Y., Cowan, S. W., and Kjeldgaard, M. (1991) *Acta Crystallogr., Sect. A 47*, 110−119.
38. Otwinowski, Z., and Minor, W. (1997) *Methods Enzymol. 276*, 307−326.
39. Graznow, R., and Reed, R. (1992) *Bio/Technology 10*, 390−393.
40. Covell, D. G., and Wallqvist, A. (1997) *J. Mol. Biol 269*, 281−297.
41. Luzzati, V. (1952) *Acta Crystallogr. 5*, 802−810.
42. Fersht, A. R. (1988) *Biochemistry 27*, 1577−1580.
43. Schreiber G,., and Fersht, A. R. (1995) *J. Mol. Biol. 248*, 478−486.
44. Fersht, A. R., Shi, J., Knill-Jones, J., Lowe, D. M., Wilkinson, A. J., Blow, D. M., Brick, P., Carter, P., Waye, M. M. Y., and Winter, G. (1985) *Nature 314*, 235−238.
45. Street, I. P., Armstrong, C. R., and Withers, S. G. (1986) *Biochemistry 25*, 6021−6027.
46. Fersht, A. R., and Serrano, L. (1993) *Curr. Opin. Struct. Biol. 3*, 75−83.
47. Levitt, M., and Perutz, M. F. (1988) *J. Mol. Biol. 201*, 751−754.
48. Serrano, L., Horovitz, A,. Avron, B., Bycroft, M., and Fersht, A. R. (1990) *Biochemistry 29*, 9343−9352.
49. LiCata, V. J., and Ackers G. K. (1995) *Biochemistry 34*, 3133−3139.
50. Horton, N., and Lewis, M. (1992) *Protein Sci. 1*, 169−181.
51. Kuntz, I. D., Meng, E. C., and Shoichet, B. K. (1994) *Acc. Chem. Res. 27*, 117−123.
52. Wallqvist, A., Jernigan, R. L., and Covell, D. G. (1995) *Protein Sci. 4*, 1881−1903.
53. Kabat, E. A., Wu, T. T., Perry, H. M., Gottesman, K. S., and Foeller, C. (1991) *Sequences of Proteins of Immunological Interest*, U. S. Public Health Service, National Institute of Health, Washington, DC.

BI980148J